Monthly Notices
of the
ROYAL ASTRONOMICAL SOCIETY

MNRAS **491,** L18–L23 (2020) doi:10.1093/mnrasl/slz154
Advance Access publication 2019 October 7

The ALPINE-ALMA [C II] survey: a triple merger at $z \sim 4.56$

G. C. Jones,[1,2]★ M. Béthermin,[3] Y. Fudamoto,[4] M. Ginolfi,[4] P. Capak,[5] P. Cassata,[6] A. Faisst,[5] O. Le Fèvre,[3]★ D. Schaerer,[4] J. D. Silverman,[7,8] Lin Yan,[9] S. Bardelli,[10] M. Boquien,[11] A. Cimatti,[12,13] M. Dessauges-Zavadsky,[4] M. Giavalisco,[14] C. Gruppioni,[10] E. Ibar,[15] Y. Khusanova,[3] A. M. Koekemoer,[16] B. C. Lemaux,[17] F. Loiacono,[10,12] R. Maiolino,[1,2] P. A. Oesch,[4,18] F. Pozzi,[10] D. Riechers,[19,20]† G. Rodighiero,[6] M. Talia,[10,12] L. Vallini,[21] D. Vergani,[10] G. Zamorani[10] and E. Zucca[10]

Affiliations are listed at the end of the paper

Accepted 2019 October 3. Received 2019 October 2; in original form 2019 August 21

ABSTRACT

We report the detection of [C II] λ158 μm emission from a system of three closely separated sources in the Cosmic Evolution Survey (COSMOS) field at $z \sim 4.56$, as part of the Atacama Large Millimeter/submillimeter Array (ALMA) Large Program to INvestigate C II at Early times (ALPINE). The two most luminous sources are closely associated, both spatially (1.6 arcsec $\sim$ 11 kpc) and in velocity ($\sim$100 km s^{-1}), while the third source is slightly more distant (2.8 arcsec $\sim$ 18 kpc, $\sim$300 km s^{-1}). The second most luminous source features a slight velocity gradient, while no significant velocity gradient is seen in the other two sources. Using the observed [C II] luminosities, we derive a total $\log_{10}(\mathrm{SFR}_{[\mathrm{C\,II}]}\,[\mathrm{M}_\odot\,\mathrm{yr}^{-1}]) = 2.8 \pm 0.2$, which may be split into contributions of 59, 31, and 10 per cent from the central, east, and west sources, respectively. Comparison of these [C II] detections to recent zoom-in cosmological simulations suggests an ongoing major merger. We are thus witnessing a system in a major phase of mass build-up by merging, including an ongoing major merger and an upcoming minor merger, which is expected to end up in a single massive galaxy by $z \sim 2.5$.

Key words: galaxies: evolution – galaxies: high-redshift – galaxies: interactions – galaxies: kinematics and dynamics.

1 INTRODUCTION

Cosmological zoom-in simulations of high-redshift galaxies (i.e. $z > 4$) show that they built up mass through a complex process, with both continuous gas accretion from diffuse haloes and discrete episodes of major and minor mergers (e.g. Vallini et al. 2013; Pallottini et al. 2017, 2019; Kohandel et al. 2019).

While secular accretion is difficult to directly observe due to its low-excitation nature, observational evidence of merging at these high redshifts is pervasive. The brightest examples of such merging are galaxies undergoing bursts in star formation apparently driven by major mergers (e.g. Oteo et al. 2016; Riechers et al. 2017; Marrone et al. 2018; Pavesi et al. 2018). In addition, resolved spectral observations have revealed evidence of merging in star-forming main-sequence galaxies (SFGs; e.g. Noeske et al. 2007; Speagle et al. 2014), or galaxies whose stellar masses and star formation rate show a correlation, with a normalization that evolves with redshift. This evidence of merging is manifest as a clumpy morphology (Ouchi et al. 2013; Riechers et al. 2014; Capak et al. 2015; Maiolino et al. 2015; Willott et al. 2015; Barisic et al. 2017; Carniani et al. 2017, 2018a,b; Jones et al. 2017; Matthee et al. 2017, 2019; Ribeiro et al. 2017), which is interpreted as ongoing galaxy assembly via minor mergers. The presence of clumps may also be explained by gravitational instabilities inside disc galaxies (e.g. Agertz, Teyssier & Moore 2009), and the true nature of a source may only be revealed using detailed kinematic information (e.g. from spectroscopy). Despite the number of individual detections, the sample of observed mergers at $z > 4$ confirmed from dynamical arguments is still statistically low, and more detections are required in order to characterize the merger rate as a function of cosmological time at these high redshifts.

The need for a more systematic merger identification and characterization at $z > 4$ can be fulfilled by the Atacama Large Mil-

---

★ E-mail: gj283@cam.ac.uk (GCJ), olivier.lefevre@lam.fr (OLF)
† Humboldt Research Fellow.

Published by Oxford University Press on behalf of the Royal Astronomical Society

limeter/submillimeter Array (ALMA) Large Program to INvestigate C II at Early times (ALPINE; Faisst et al. 2019; Le Fèvre et al. in preparation), which observed [C II] λ158 μm emission and rest frame ∼158 μm continuum emission from 118 SFGs in the Cosmic Evolution Survey (COSMOS) and *Extended Chandra Deep Field-South* (ECDF-S) fields with $4.4 < z_{\rm spec} < 5.8$, SFR > 10 M$_\odot$ yr^{-1}, $\log(M_*/{\rm M}_\odot) = 9$–11, and $L_{\rm UV} > 0.6\,L^*$. These cuts were made to ensure that the sample represents the overall galaxy population at this epoch.

Since [C II] is generally the brightest far-infrared (FIR) emission line for star-forming galaxies (Carilli & Walter 2013) and is emitted from all the gas phases (ionized, neutral, and molecular) of the interstellar medium (ISM; Pineda et al. 2013), it is a prime tracer of the gas kinematics of high-redshift galaxies. As an example of mergers identified in the ALPINE survey, we detail here the detection of [C II] and dust continuum emission from the $z_{\rm [C\,II]} = 4.56$ dusty triple merger DEIMOS_COSMOS_818760 (hereafter DC 818760).

Because it is located in the well-studied COSMOS field (Scoville et al. 2007a,b), DC 818760 has been observed with a number of near-ultraviolet (NUV)–NIR instruments, including *Hubble Space Telescope* (*HST*), Subaru, and *Spitzer* (Laigle et al. 2016). Using the broad-band [i.e. Canada–France–Hawaii Telescope (CFHT) *u* through *Spitzer* Infrared Array Camera (IRAC) 8.0 μm] spectral energy distribution (SED) of DC 818760 and the SED modelling code LePhare (Arnouts et al. 1999; Ilbert et al. 2006; Arnouts & Ilbert 2011) with a Chabrier initial mass function and Calzetti starburst extinction law, Faisst et al. (in preparation) find a stellar mass of $\log(M_*\,[{\rm M}_\odot]) = 10.6 \pm 0.1$ and a star formation rate $\log({\rm SFR}\,[{\rm M}_\odot\,{\rm yr}^{-1}]) = 2.7^{+0.2}_{-0.3}$. These values place DC 818760 on the upper envelope of the main sequence at $z \sim 4.6$ (Speagle et al. 2014; Tasca et al. 2015).

In addition, DC 818760 is in close proximity (i.e. ∼5.5 proper Mpc and <500 km s^{-1}) to the massive protocluster PC1 J1001+0220 (Lemaux et al. 2018). Since it lies along the major axis of the protocluster, and is only ∼3.5 proper Mpc from the north-east component of this protocluster, DC 818760 may be associated with the system in a filamentary structure.

In this work, we discuss new ALMA observations of [C II] and submm continuum emission from DC 818760 obtained as part of the ALMA large program ALPINE, and examine its triple merger nature. We assume a flat Λ cold dark matter (ΛCDM) cosmology ($\Omega_\Lambda = 0.7$, $\Omega_{\rm m} = 0.3$, $H_0 = 70$ km s^{-1}) throughout. At the redshift of DC 818760 ($z_{\rm [C\,II]} = 4.560$), 1 arcsec corresponds to 6.563 proper kpc.

2 OBSERVATIONS AND DATA REDUCTION

The [C II] emission from DC 818760 was observed with ALMA on 2018 May 25 in cycle 5 (project 2017.1.00428.L, PI: O. Le Fèvre) using configuration C43-2 (baselines ∼15–320 m), 45 antennas, and an on-source time of 17 min. J0158+0133 was used as a bandpass and flux calibrator, while J0948+0022 was used as a phase calibrator.

The spectral set-up consisted of two sidebands, each constructed of two spectral windows (SPWs) of width 1.875 GHz. Each SPW was made of channels of width 15.625 MHz. The lower sideband is tuned to the redshifted [C II] frequency, while the upper sideband is solely used for continuum.

Calibration was performed using the heuristic-based CASA 5.4.1 automatic pipeline, with reduced automatic band-edge channel flagging (Béthermin et al. in preparation). The pipeline calibration diagnostics were inspected carefully and no issues were found. To maximize sensitivity, we adopted natural weighting.

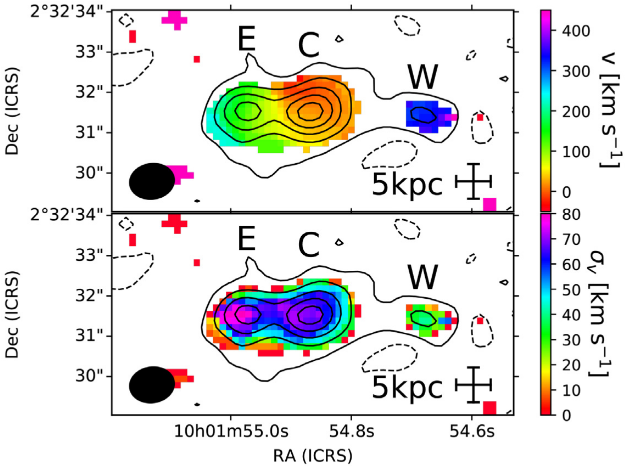

Figure 1. Total [C II] moment zero map (contours), velocity field (top colour), and velocity dispersion map (bottom colour). Contours begin at $\pm 2\sigma$, where $1\sigma = 0.1$ Jy beam^{-1} km s^{-1}, and are in steps of 5σ. Zero velocity is defined as $z_{\rm [C\,II]} = 4.560$, or the redshift of the central source. The synthesized beam (1.07×0.84 arcsec^2, with major axis position angle $= -82°$) is shown by the solid black ellipse to the lower left. A 5 ×5 kpc^2 scale is shown in the lower right. North is up and east is to the left.

Continuum and line emission were separated using the CASA task UVCONTSUB. The lower sideband was made into a data cube using the CASA task TCLEAN, resulting in an average rms noise level per 15.625 MHz (∼14 km s^{-1}) channel of 0.6 mJy beam^{-1} and a synthesized beam of 1.07×0.84 arcsec^2 at $-81°$. To maximize sensitivity, one continuum image was created using all line-free data in both sidebands using TCLEAN in multifrequency synthesis mode. This results in a continuum image with an rms noise level of 0.05 mJy beam^{-1} and the same synthesized beam as the upper sideband.

3 IMAGING RESULTS

In order to investigate the [C II] emission in this source, we first examine which channels show emission with $>2\sigma_{\rm LINE}$ ($\sigma_{\rm LINE} = 0.6$ mJy beam^{-1}). Using these channels and the CASA task IMMOMENTS, we create a moment zero image of the total [C II] emission (contours of Fig. 1). Three [C II] sources are present, all roughly at the same declination.

Using the CASA task IMFIT, we simultaneously fit three two-dimensional Gaussians to the moment zero map. The central source of this best fit (C) features an integrated flux density (4.9 ± 0.3) Jy km s^{-1}, a peak flux density (2.4 ± 0.1) Jy beam^{-1} km s^{-1}, and a beam-deconvolved size $(1.2 \pm 0.1) \times (0.8 \pm 0.1)$ arcsec^2 at a position angle ($111° \pm 11°$), defined counterclockwise from north. The second source (E), which is 1.6 arcsec (∼11 kpc) to the east of source C, shows an integrated flux density (2.6 ± 0.2) Jy km s^{-1}, a peak flux density (1.9 ± 0.1) Jy beam^{-1} km s^{-1}, and a deconvolved size $(0.8 \pm 0.1) \times (0.3 \pm 0.2)$ arcsec^2 at a position angle ($9° \pm 169°$). Lastly, the weakest source (W), which is 2.8 arcsec (∼18 kpc) west of source C, has an integrated flux density (0.8 ± 0.2) Jy km s^{-1}, a peak flux density (0.9 ± 0.1) Jy beam^{-1} km s^{-1}, and is unresolved.

The kinematics of this field are revealed by the velocity field (moment one image), created using the CASA task IMMOMENTS (top

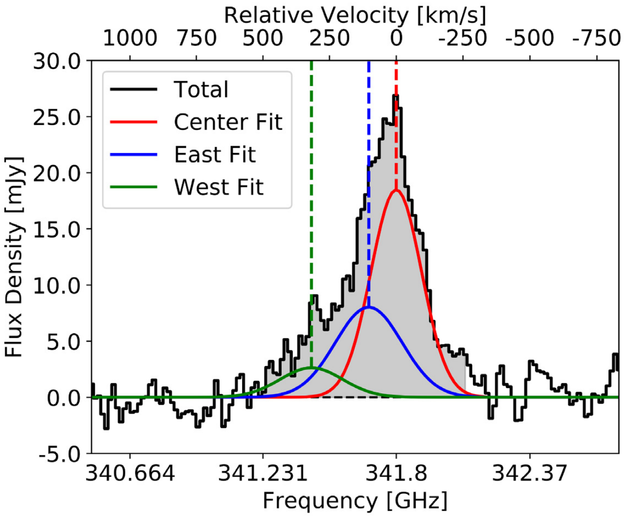

Figure 2. Global spectrum taken over 2σ contour of total [C II] moment zero map (black histogram). Shaded region shows channels used to create moment zero image (contours of Fig. 1). An approximation of the contribution of each source is shown by solid coloured lines, with the central frequency marked by a vertical dashed line of the same colour.

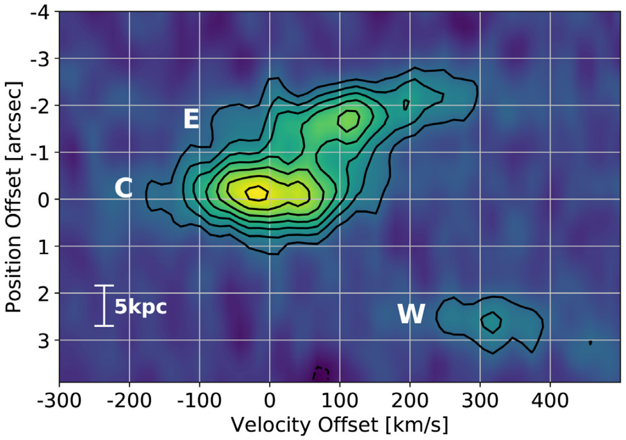

Figure 3. Position–velocity diagram taken east–west, centred on the central source, with a total width of 8 arcsec and an averaging width of 5 pixels. Contours begin at 3σ, where $1\sigma = 0.6$ mJy beam^{-1}, and are in steps of 2σ. East is up and west is down. Scale of 5 kpc shown to lower left.

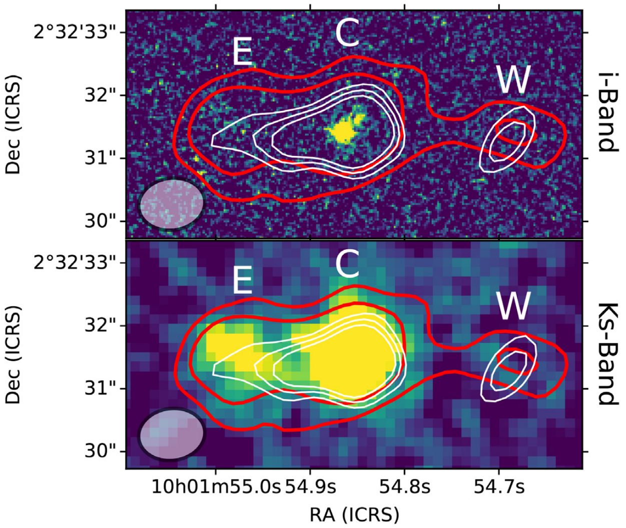

Figure 4. Background image of the top panel shows *HST*/Advanced Camera for Surveys (ACS) *F814W* (*i*-band) image of DC 818760 (Koekemoer et al. 2007; Scoville et al. 2007b), while the bottom panel shows the UltraVISTA K_s-band image (DR4; McCracken et al. 2012). In both panels, white contours depict the continuum image created using all line-free data. Contours shown at 3σ, 4σ, and 5σ, where $1\sigma = 0.05$ mJy beam^{-1}. The synthesized beam (1.06×0.82 arcsec^2, with major axis position angle $= -82°$) is shown by the solid black ellipse to the lower left. For reference, the $(3,7)\sigma$ [C σ] moment zero contours are shown in red. North is up and east is to the left.

panel colour of Fig. 1). While the two brightest sources (i.e. C and E) are only separated by $\sim$100 km s^{-1}, source W is $\sim$300 km s^{-1} offset from source C. Sources C and W show nearly constant velocity, while source E shows a strong gradient (50–200 km s^{-1}).

The IMMOMENTS task may also be used to create a velocity dispersion (moment two) map (bottom panel colour of Fig. 1). Source W shows a relatively low velocity dispersion ($\sigma_{v,\,\mathrm{W,\,pk}} \sim$ 40 km s^{-1}), while sources C and E exhibit strong peaks in velocity dispersion ($\sigma_{v,\,\mathrm{C,\,pk}} \sim$ 70 km s^{-1}, $\sigma_{v,\,\mathrm{E,\,pk}} \sim$ 80 km s^{-1}). These σ_v peaks may be artificially enhanced by beam smearing (e.g. Weiner et al. 2006), but each is spatially coincident with a [C II] source.

Extracting a spectrum over the 2σ contour of the moment zero map, which contains all three sources, we obtain the profile shown in Fig. 2 (black line). To determine the contribution of each source, we first assign each spaxel within the 2σ moment zero contour to one of the three sources, based on the relative contributions of each of the three Gaussian components output from CASA IMFIT. The corresponding pixels for each source are then integrated to produce three integrated spectra. For clarity, each spectrum is fit with a one-dimensional Gaussian, and displayed in Fig. 2, along with its centroid velocity. We find that sources E and W are both redshifted with respect to source C by 103 ± 6 and 318 ± 5 km s^{-1}, respectively. The redshift of the dominant source C, which will be used as the redshift of this field, is 4.56038 ± 0.00004.

To examine the kinematics of this system in another way, we create a position–velocity (PV) diagram (CASA IMPV) by extracting a 5 pixel thick (1 pixel = 0.16 arcsec), 8 arcsec long slice across the right ascension axis of the data cube, centred on the central source. This 3D slice was then averaged in declination to create a single intensity plane (see Fig. 3). This PV diagram confirms that both of the fainter sources (i.e. E and W) are moving at positive velocities with respect to source C, as seen in the spectra (Fig. 2). While the sources C and E are closely connected, the source C and W are separated by $\sim$18 kpc and $\sim$300 km s^{-1} .

In addition to [C II] emission, dust continuum emission is detected at the location of all three sources (white contours of Fig. 4). While the [C II] emission features three distinct peaks, the bulk of the continuum emission is concentrated in source C, with a strong extension to the east, and a 4σ component coincident with source W. A single component, two-dimensional Gaussian fit to the combined emission of the source C and its eastern extension using CASA IMFIT yields a peak flux density of 0.44 ± 0.05 mJy beam^{-1}, an integrated flux density of 1.22 ± 0.18 mJy, and a deconvolved size of $(1.95 \pm 0.35) \times (0.71 \pm 0.18)$ arcsec^2 at $(90° \pm 7°)$. The continuum emission from source W is unresolved, with a peak flux density of 0.18 ± 0.05 mJy beam^{-1} and integrated flux density of 0.26 ± 0.11 mJy.

Table 1. Observed and derived quantities for each source in DC 818760, the combined quantities of the central and eastern sources, and the combined quantities of all three sources. Positional uncertainty is ∼0.15 arcsec. $\mathrm{SFR}_{[\mathrm{C\,II}]}$ is derived from $L_{[\mathrm{C\,II}]}$ using the full SFG relation of De Looze et al. (2014).

	C	E	W	CE	CEW
Right ascension	$10^{\mathrm{h}}01^{\mathrm{m}}54\overset{\mathrm{s}}{.}865$	$10^{\mathrm{h}}01^{\mathrm{m}}54\overset{\mathrm{s}}{.}978$	$10^{\mathrm{h}}01^{\mathrm{m}}54\overset{\mathrm{s}}{.}683$	…	…
Declination	$+2^\circ32'31\overset{''}{.}53$	$+2^\circ32'31\overset{''}{.}50$	$+2^\circ32'31\overset{''}{.}44$	…	…
$z_{[\mathrm{C\,II}]}$	4.56038 ± 0.00004	4.56229 ± 0.00008	4.56628 ± 0.00014	…	…
$S\Delta v_{[\mathrm{C\,II}]}$ (Jy km s^{-1})	4.9 ± 0.3	2.6 ± 0.2	0.8 ± 0.2	7.5 ± 0.4	8.3 ± 0.4
S_{cont} (mJy)	…	…	0.26 ± 0.11	1.22 ± 0.18	1.48 ± 0.21
$\log L_{[\mathrm{C\,II}]}$ (L$_\odot$)	9.48 ± 0.03	9.21 ± 0.03	8.70 ± 0.11	9.67 ± 0.02	9.7 ± 0.02
$\log \mathrm{SFR}_{[\mathrm{C\,II}]}$ (M$_\odot$ yr^{-1})	2.59 ± 0.24	2.31 ± 0.23	1.80 ± 0.25	2.77 ± 0.24	2.82 ± 0.23

The *HST*/Advanced Camera for Surveys (ACS) *F814W* (*i*-band) image of this source reveals emission from only source C. This emission may be decomposed into two components separated by only ∼0.3 arcsec (1.9 kpc), possibly indicating a small-separation merger or an inhomogeneous dust screen. Higher resolution ALMA [C II] observations are required to determine the nature of this double detection in C. On the other hand, the UltraVISTA K_{s}-band image of this field shows emission from both source C and E. Neither image shows significant emission from source W. We note that the *i*- and K_{s}-band images have different point spread functions (PSFs; i.e. 0.09 and 0.65 arcsec), and that the K_{s}-band image is ∼2 orders of magnitude less sensitive than the *i*-band image, based on 5σ point-source sensitivities. Since the three components of DC 818760 are spatially separated, and the more sensitive image shows fewer detections, these differences are not responsible for the non-detections. This dramatic increase in the emission between the *i* band ($\lambda_{\mathrm{rest}} \sim 1450$ Å) and K_{s} band ($\lambda_{\mathrm{rest}} \sim 4000$ Å) for source E may indicate a steep ultraviolet (UV) slope, implying a significant dust presence (e.g. Calzetti et al. 2000).

4 ANALYSIS

4.1 Star formation rate

The empirical $L_{[\mathrm{C\,II}]}$ to SFR calibration of De Looze et al. (2014) for their full sample of star-forming galaxies may be used to estimate the SFR of each source individually. We note that Carniani et al. (2018a) found that a sample of $z > 5$ [C II] star-forming galaxies featured a ∼2× larger dispersion in this relation than is stated in De Looze et al. (2014) for local galaxies, so the resulting uncertainties in SFR for DC 818760 are likely slightly underestimated. The three $L_{[\mathrm{C\,II}]}$-derived SFRs (see Table 1) sum to $\log_{10}(\mathrm{SFR}_{[\mathrm{C\,II}]}\,[\mathrm{M}_\odot\,\mathrm{yr}^{-1}]) = 2.82 \pm 0.23$. Comparing the different sources, we find that the star formation activity of the system may be split into contributions from source C (59 per cent), E (31 per cent), and W (10 per cent).

Using flux densities extracted from an aperture centred on source C of diameter 3 arcsec, which encloses only source C and a portion of source E, Faisst et al. (in preparation) created a broad-band SED of DC 818760, and fit it with LEPHARE. The resulting value of $\log_{10}(\mathrm{SFR}_{\mathrm{SED}}\,[\mathrm{M}_\odot\,\mathrm{yr}^{-1}]) = 2.7^{+0.2}_{-0.3}$ is in agreement with our value for the source C of $\log_{10}(\mathrm{SFR}_{[\mathrm{C\,II}],\mathrm{C}}\,[\mathrm{M}_\odot\,\mathrm{yr}^{-1}]) = 2.59 \pm 0.24$, suggesting that [C II] is an appropriate SFR tracer in this source.

4.2 Comparison to simulations

The recent zoom-in cosmological simulations of Kohandel et al. (2019) detail the evolution of a disc galaxy (‘Althæa’) undergoing minor and major merger events between $z = 7.21$ and 6.09, and give both face-on and edge-on spectra for several evolutionary stages. In order to further characterize DC 818760, we compare our [C II] observations with the results of these simulations.

First, the global spectrum of DC 818760 (Fig. 2) shows an asymmetric Gaussian, composed of the dominant source C and the slightly weaker source E. This feature is also seen in the face-on merger spectrum of Althæa (fig. 6 of Kohandel et al. 2019). This similarity supports the merger interpretation of these two sources.

In addition, Kohandel et al. (2019) highlight the fact that galaxies with narrow spectral profiles (i.e. face-on discs, dispersion-dominated systems) are more easily observed than galaxies whose emission is spread over a broad velocity range (i.e. edge-on discs, mergers), due to their high peak flux density. This implies that additional components of the DC 818760 system may also be present, but are too faint to be detected in our current observation. Indeed, the simulated galaxy Dahlia ($z \sim 6$, SFR ∼ 100 M$_\odot$ yr^{-1}; Pallottini et al. 2017) features 14 satellite clumps within 100 kpc of its central galaxy, but only three of them were detected in [C II] emission in a simulated observation. Thus, the DC 818760 system is likely more complex than the three sources that we observe.

5 CONCLUSIONS

In this Letter, we have presented the detection of [C II] emission from three sources in the field DC 818760, as observed with ALMA as part of the large program ALPINE. The two dominant sources (C and E) are closely associated, both spatially (1.6 arcsec ∼ 11 kpc) and in velocity (∼100 km s^{-1}), while the third source (W) is separate (2.8 arcsec ∼ 18 kpc, ∼300 km s^{-1}). Source E features a strong velocity gradient, which may either suggest a rotating galaxy or a tidally disrupted galaxy, while the others exhibit nearly constant velocity. All three show velocity dispersion peaks coincident with the peak of [C II] emission. Because of their kinematical properties, we conclude that the three sources in this field are separate objects, not members of the same galaxy.

The close spatial separation, low velocity offset, and similar [C II] luminosities ($L_{[\mathrm{C\,II}],\,\mathrm{C}}/L_{[\mathrm{C\,II}],\,\mathrm{E}} = 1.86 < 4$) of sources C and E suggest an ongoing major merger (Lotz et al. 2011). Dynamical arguments from merger simulations (e.g. Kitzbichler & White 2008) indicate that these two sources will merge within <0.5 Gyr. On the other hand, sources C and W are spatially and kinematically separate, but only by ∼18 kpc and ∼300 km s^{-1}. This close separation and their large luminosity ratio ($L_{[\mathrm{C\,II}],\,\mathrm{C}}/L_{[\mathrm{C\,II}],\,\mathrm{W}} = 6.03 > 4$) suggest that they will coalesce in a minor merger at a later time.

Based on both rest-frame UV observations and FIR continuum detections, there is strong evidence for significant internal extinction. Regarding the former, DC 818760 was originally targeted with DEep Imaging Multi-Object Spectrograph (DEIMOS; Hasinger et al. 2018) using a slit coincident only with the central source.

Lyα emission was not detected, but rather only UV ISM absorption lines, which strengthens the argument for dust obscuration.

Using the observed [C II] luminosities, we derive a total $\log_{10}(\mathrm{SFR}\,[\mathrm{M}_{\odot}\,\mathrm{yr}^{-1}]) = 2.8 \pm 0.2$, which may be split into 59, 31, and 10 per cent from sources C, E, and W, respectively. Comparison to cosmological zoom-in simulations shows that the two dominant components resemble a merger and that the field likely contains multiple undetected sources.

We are thus witnessing a massive galaxy in the early phase of mass assembly with merging playing a major role. This system contains three kinematically distinct components: two currently undergoing a major merger (i.e. C and E), and a third minor component that will likely merge with the other two in the future (i.e. W). While the example given by this system is striking, larger samples are needed in order to assess how frequent such systems may be. The ALPINE sample is providing the opportunity to acquire a robust statistical knowledge of normal star-forming galaxies undergoing rapid mass growth, as will be presented in forthcoming papers.

ACKNOWLEDGEMENTS

This Letter is based on data obtained with the ALMA Observatory, under Large Program 2017.1.00428.L. ALMA is a partnership of ESO (representing its member states), NSF (USA), and NINS (Japan), together with NRC (Canada), MOST and ASIAA (Taiwan), and KASI (Republic of Korea), in cooperation with the Republic of Chile. The Joint ALMA Observatory is operated by ESO, AUI/NRAO, and NAOJ. Based on data products from observations made with ESO Telescopes at the La Silla Paranal Observatory under ESO programme ID 179.A-2005, on data products produced by TERAPIX, and the Cambridge Astronomy Survey Unit on behalf of the UltraVISTA consortium. This program is supported by the national program Cosmology and Galaxies from the CNRS in France. GCJ and RM acknowledge ERC Advanced Grant 695671 'QUENCH' and support by the Science and Technology Facilities Council (STFC). DR acknowledges support from the National Science Foundation under grant number AST-1614213 and from the Alexander von Humboldt Foundation through a Humboldt Research Fellowship for Experienced Researchers. AC, FP, and MT acknowledge the grant MIUR PRIN2017. LV acknowledges funding from the European Union's Horizon 2020 research and innovation program under the Marie Sklodowska-Curie grant agreement no. 746119. EI acknowledges partial support from FONDECYT through grant N° 1171710.

REFERENCES

Agertz O., Teyssier R., Moore B., 2009, MNRAS, 397, L64
Arnouts S., Ilbert O., 2011, Astrophysics Source Code Library. record ascl:1108.009
Arnouts S., Cristiani S., Moscardini L., Matarrese S., Lucchin F., Fontana A., Giallongo E., 1999, MNRAS, 310, 540
Barisic I. et al., 2017, ApJ, 845, 41
Calzetti D., Armus L., Bohlin R. C., Kinney A. L., Koornneef J., Storchi-Bergmann T., 2000, ApJ, 533, 682
Capak P. L. et al., 2015, Nature, 522, 455
Carilli C. L., Walter F., 2013, ARA&A, 51, 105
Carniani S. et al., 2017, A&A, 605, A42
Carniani S. et al., 2018a, MNRAS, 478, 1170
Carniani S., Maiolino R., Smit R., Amorín R., 2018b, ApJ, 854, L7
De Looze I. et al., 2014, A&A, 568, A62
Faisst A., Bethermin M., Capak P., Cassata P., LeFevre O., Schaerer D., Silverman J., Yan L., 2019, preprint (arXiv:1901.01268)
Hasinger G. et al., 2018, ApJ, 858, 77
Ilbert O. et al., 2006, A&A, 457, 841
Jones G. C., Willott C. J., Carilli C. L., Ferrara A., Wang R., Wagg J., 2017, ApJ, 845, 175
Kitzbichler M. G., White S. D. M., 2008, MNRAS, 391, 1489
Koekemoer A. M. et al., 2007, ApJS, 172, 196
Kohandel M., Pallottini A., Ferrara A., Zanella A., Behrens C., Carniani S., Gallerani S., Vallini L., 2019, MNRAS, 487, 3007
Laigle C. et al., 2016, ApJS, 224, 24
Lemaux B. C. et al., 2018, A&A, 615, A77
Lotz J. M., Jonsson P., Cox T. J., Croton D., Primack J. R., Somerville R. S., Stewart K., 2011, ApJ, 742, 103
McCracken H. J. et al., 2012, A&A, 544, A156
Maiolino R. et al., 2015, MNRAS, 452, 54
Marrone D. P. et al., 2018, Nature, 553, 51
Matthee J. et al., 2017, ApJ, 851, 145
Matthee J. et al., 2019, ApJ, 881, 124
Noeske K. G. et al., 2007, ApJ, 660, L43
Oteo I. et al., 2016, ApJ, 827, 34
Ouchi M. et al., 2013, ApJ, 778, 102
Pallottini A., Ferrara A., Gallerani S., Vallini L., Maiolino R., Salvadori S., 2017, MNRAS, 465, 2540
Pallottini A. et al., 2019, MNRAS, 487, 1689
Pavesi R. et al., 2018, ApJ, 861, 43
Pineda J. L., Langer W. D., Velusamy T., Goldsmith P. F., 2013, A&A, 554, A103
Ribeiro B. et al., 2017, A&A, 608, A16
Riechers D. A. et al., 2014, ApJ, 796, 84
Riechers D. A. et al., 2017, ApJ, 850, 1
Scoville N. et al., 2007a, ApJS, 172, 1
Scoville N. et al., 2007b, ApJS, 172, 38
Speagle J. S., Steinhardt C. L., Capak P. L., Silverman J. D., 2014, ApJS, 214, 15
Tasca L. A. M. et al., 2015, A&A, 581, A54
Vallini L., Gallerani S., Ferrara A., Baek S., 2013, MNRAS, 433, 1567
Weiner B. J. et al., 2006, ApJ, 653, 1027
Willott C. J., Carilli C. L., Wagg J., Wang R., 2015, ApJ, 807, 180

[1] *Cavendish Laboratory, University of Cambridge, 19 J. J. Thomson Ave., Cambridge CB3 0HE, UK*
[2] *Kavli Institute for Cosmology, University of Cambridge, Madingley Road, Cambridge CB3 0HA, UK*
[3] *Aix Marseille Univ, CNRS, Laboratoire d'Astrophysique de Marseille (LAM), Marseille 13013, France*
[4] *Observatoire de Genève, Université de Genève, 51 Chemin des Maillettes, CH-1290 Versoix, Switzerland*
[5] *IPAC, California Institute of Technology, 1200 East California Boulevard, Pasadena, CA 91125, USA*
[6] *Department of Physics and Astronomy, University of Padova, Vicolo Osservatorio 3, I-35122 Padova, Italy*
[7] *Kavli Institute for the Physics and Mathematics of the Universe, The University of Tokyo, Kashiwa 277-8583, Japan*
[8] *Department of Astronomy, School of Science, The University of Tokyo, 7-3-1 Hongo, Bunkyo, Tokyo 113-0033, Japan*
[9] *Caltech Optical Observatories, Cahill Center for Astronomy and Astrophysics, 1200 East California Boulevard, Pasadena, CA 91125, USA*
[10] *Istituto Nazionale di Astrofisica – Osservatorio di Astrofisica e Scienza dello Spazio, via Gobetti 93/3, I-40129 Bologna, Italy*
[11] *Centro de Astronomía (CITEVA), Universidad de Antofagasta, Avenida Angamos 601, Antofagasta, Chile*
[12] *Department of Physics and Astronomy (DIFA), University of Bologna, via Gobetti 93/2, I-40129 Bologna, Italy*
[13] *INAF – Osservatorio Astrofisico di Arcetri, Largo E. Fermi 5, I-50125 Firenze, Italy*
[14] *Department of Physics and Astronomy, University of Massachusetts, Amherst, MA 01003, USA*

[15] *Instituto de Física y Astronomía, Universidad de Valparaíso, Avda. Gran Bretaña 1111, Valparaíso, Chile*
[16] *Space Telescope Science Institute, 3700 San Martin Dr., Baltimore, MD 21218, USA*
[17] *Department of Physics, University of California, Davis, One Shields Ave., Davis, CA 95616, USA*
[18] *International Associate, Cosmic Dawn Center (DAWN) at the Niels Bohr Institute, University of Copenhagen and DTU-Space, Technical University of Denmark, Copenhagen, Denmark*
[19] *Department of Astronomy, Cornell University, Space Sciences Building, Ithaca, NY 14853, USA*
[20] *Max-Planck-Institut für Astronomie, Königstuhl 17, D-69117 Heidelberg, Germany*
[21] *Leiden Observatory, Leiden University, PO Box 9500, NL-2300 RA Leiden, the Netherlands*

This paper has been typeset from a TEX/LATEX file prepared by the author.